

Dirac node lines in pure alkali earth metals

Ronghan Li¹, Xiyue Cheng¹, Ma Hui¹, Shoulong Wang¹, Dianzhong Li¹, Zhengyu Zhang², Yiyi Li¹, and Xing-Qiu Chen^{1*}

¹Shenyang National Laboratory for Materials Science, Institute of Metal Research, Chinese Academy of Science, 110016 Shenyang, Liaoning, China and

²International Center for Quantum Design of Functional Materials (ICQD), Hefei National Laboratory for Physical Sciences at the Microscale (HFNL) and Synergetic Innovation Center of Quantum Information and Quantum Physics, University of Science and Technology of China, Hefei, Anhui 230026, P. R. China

(Dated: March 4, 2024)

Beryllium is a simple alkali earth metal, but has been the target of intensive studies for decades because of its unusual electron behaviors at surfaces. Puzzling aspects include (i) severe deviations from the description of the nearly free electron picture, (ii) anomalously large electron-phonon coupling effect, and (iii) giant Friedal oscillations. The underlying origins for such anomalous surface electron behaviors have been under active debate, but with no consensus. Here, by means of first-principle calculations, we discover that this pure metal system, surprisingly, harbors the Dirac node line (DNL) that in turn helps to rationalize many of the existing puzzles. The DNL is featured by a closed line consisting of linear band crossings and its induced topological surface band agrees well with previous photoemission spectroscopy observation on Be (0001) surface. We further reveal that each of the elemental alkali earth metals of Mg, Ca, and Sr also harbors the DNL, and speculate that the fascinating topological property of DNL might naturally exist in other elemental metals as well.

Topological semimetals[1] represent new types of quantum matter, currently attracting widespread interest in condensed matter physics and materials science. Compared with normal metals, topological semimetals are distinct in two essential aspects: the crossing points of the energy bands occur at the Fermi level, and some of the crossing points consist of the monopoles in the lattice momentum space. Topological semimetals can be classified into three main categories, topological Dirac (TD)[2], topological Weyl (TW)[3] and Dirac node line (DNL) semimetals[4–6], respectively. In the former two cases of TD and TW, the monopoles form isolated points in lattice momentum space and novel surface states (i.e., surface Dirac cones and Fermi-arc states) were observed or suggested, such as TD-type Na₃Bi[7–10] and Cd₃As₂[11–13] and TW-type TaAs-family[14–17] and TW-type-II WTe₂[18].

In the third class of DNL, the crossings between energy bands form a fully closed line nearly at the Fermi level in the lattice momentum space, drastically different from the isolated Dirac (or Weyl) points in the TD and TW. The projection of the Dirac node line into a certain surface would result in a closed ring in which the topological surface states (usually flat bands) can be expected to appear due to the non-trivial topological property of its bulk phase. According to the previous DNL modelings[4, 5], the band crossings occur at zero energy with a constraint chiral symmetry, leading to the appearance of flat topologically protected surface bands. However, in a real crystal the chiral symmetry of a band structure is not exact, thereby suggesting that the DNL does not generally occur at a constant energy and the DNL-induced topological surface bands are not flat either. Recently, this type of DNL states has been predicted in several cases of 3D carbon graphene allotropes[19], antiperovskite Cu₃(Pd,Zn)N[20, 21], Ca₃P₂[22], LaN[23], photonic crystals[24] and a hyperhoneycomb lattice[25], etc. But, all these DNL predictions have yet to be experimentally verified. Here, we discover a new DNL

state in beryllium, the first known example in pure metals. We find that the presence of the topologically protected (0001) surface states around the $\bar{\Gamma}$ point originates from this DNL state. Furthermore, realization of the existence of the DNL in principle offers new opportunities and insights in rationalizing the long-standing problem[26–34] of the pronounced surface states in Be.

The metal of beryllium, which crystallizes in the hcp structure (see Fig. 1a), is a simple *sp*-bonded metal. Be is unusual in three aspects. Firstly, at its bulk phase it is almost a semimetal, whereas its (0001) surface has the well-defined, intense and robust surface electronic states[26–28]. Here, the surface density of state at the Fermi level is almost five times higher than that of its bulk phase[26, 33, 34]. The surface states of simple metals were often interpreted within the framework of the nearly-free-electron model[26], however beryllium behaves surprisingly far beyond this model. Secondly, the anomalous interplanar expansion[32] as large as > 4% of the topmost (0001) atomic layer has been observed, different from most other pure metals which often show little relaxations or contractions when cracking into surface. The underlying driving force for the lattice expansion has again been attributed to unusual electronic states at the surfaces[35, 36]. Thirdly, the large electron-phonon coupling ($\lambda = 1.18$)[30] and giant Friedal oscillations[31] have been found at its (0001) surface. This fact along with the high density of states at the Fermi level was suggested to be a candidate to show surface superconductivity[29].

We start by representing the electronic structure of the bulk hcp Be phase (Fig. 1a) at the ground state within the framework of density functional theory (DFT) (Supplementary Materials). The derived electronic band structure of the hcp Be is shown in Fig. 1c. It is quite similar to previous calculations[37]. We also derive the Fermi surface of its bulk phase in Fig. 2a, in a nice accordance with the experimen-

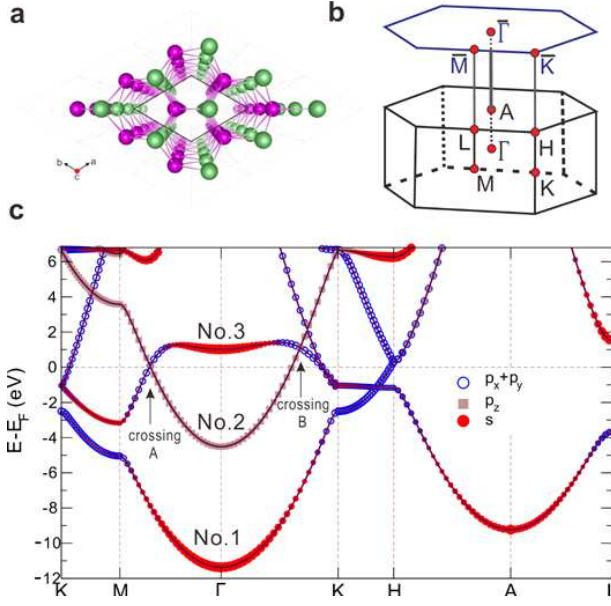


FIG. 1: **Lattice structure and electronic band structure of hcp beryllium.** **a**, Crystal structure (here a $3 \times 3 \times 5$ supercell) (No.194 P63/mmc space group) with Be atom at 2c site (1/3, 2/3, 1/4) in a perspective projection along the c-axis. The layers consisting of green and pink atoms alternatively stack along c-axis. **b**, Brillouin zone (BZ) of the bulk phase and projected surface BZ of the (0001) surface, **c** Calculated electronic band structure along the high-symmetry points for hcp Be bulk phase.

tal measurement[38]. Its Fermi surface clearly consists of two parts: a coronet-like shape of six-cornered hole pockets on the $k_z=0$ plane, and a cigar-like shape of six equivalent electronic surfaces along the H-K symmetry direction. Nevertheless, a crucial feature was ignored in those previous studies. That is the appearance of two clear band crossings featured by a nearly linear dispersion around the Fermi level. One (crossing A) exactly locates at the Fermi level in the M- Γ direction and the other one (crossing B) lies about 0.8 eV above the Fermi level along the Γ -K direction. Actually, these two crossings are induced by the band inversion. At the centre of the Brillouin zone (BZ, see Fig. 1b), Γ , it can be seen that the band $s \rightarrow p_z$ inversion occurs between No.2 and No.3 bands due to the crystal field effect (Fig. 1c). Remarkably, the band crossings indeed not only appear at these two isolated A and B, but also form a circle-like closed line around the Γ point on the $k_z=0$ plane in BZ. This is the exact sign of the DNL appearance. As elucidated in Fig. 2b, the band crossings between No.2 and No.3 do not happen at the same energy, but show a periodic wave-like closed curve upon the k vectors around the centered Γ point. In addition, this DNL's stability is highly robust, protected by the inversion and time-reversal symmetries without the spin-orbit coupling (SOC) effect. Because of the light mass of Be, its SOC effect can be ignored.

Accordingly, we further illustrate the topology of the DNL states in Be. Since a Bloch Hamiltonian $H(\mathbf{k})$ is invariant under the inversion (P) and time-reversal (T) operations in a

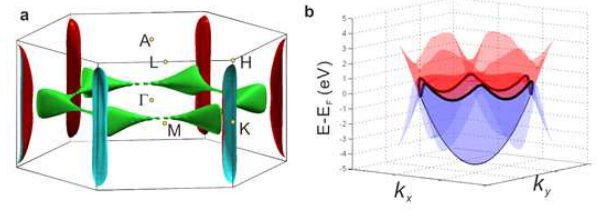


FIG. 2: **Fermi surface and the DNL in hcp Be.** **a**, The Fermi surface in bulk hcp Be exhibits two-band features: a six-cornered hole pockets around the K point in the $k_z = 0$ plane and a six column-like electronic pockets along the H-K direction. The hole pockets are perpendicular to the electronic ones in the BZ. **b**, Illustration of the DNL, highlighted by the two band crossings between the No.2 and No.3 bands near the Fermi level on the $k_z = 0$ plane for hcp Be.

centrosymmetric system without SOC, it can be inferred that $T^2=1$ and $(P \cdot T)^2=1$. The Berry phase $\gamma = \oint_C A(\mathbf{k}) d\mathbf{k}$, where $A(\mathbf{k})$ is the Berry connection of $-i \sum_n \langle u_n(\mathbf{k}) | \nabla_{\mathbf{k}} u_n(\mathbf{k}) \rangle$ and C is a closed loop in the momentum space, can be used to identify whether or not the DNL occurs[20, 21]. If the loop C is pierced by a node line, the Berry phase $\gamma = \pi$, otherwise, $\gamma = 0$. Within this relation, a Z_2 topological invariant can be introduced as $\omega(C) = \exp i\gamma$, which equals ± 1 . Following the method proposed by Fu and Kane[39], the term of $\omega(C)$ can be expressed as,

$$\omega(C_{ab}) = \xi_a \xi_b \quad (1)$$

where ξ_a is the product of the occupied band parities at a point. Using a four parity-invariant points loop[21], $C_{abcd} - C_{cd}$ to define the boundary of the surface S_{abcd} , the Z_2 invariant can count the number of node lines ($N(S)$) which pierce the surface, as reads,

$$(-1)^{N(S_{abcd})} = \omega(C_{abcd}) = \xi_a \xi_b \xi_c \xi_d \quad (2)$$

It implies that the DNL will occur around the inversion transition. Additionally, we calculate the Z_2 indices at the eight time-reversal invariant momenta (TRIMs) and obtain that the product is +1 at Γ and -1 for all the other TRIMs, as shown in TABLE I. It evidences the occurrence of a band inversion at Γ and the DNL appearance around Γ . Since the relation is very similar to the topological invariants ($\nu_0; \nu_1 \nu_2 \nu_3$) of inversion-symmetric topological insulator[39]. The Z_2 invariant in Be can be written as (1; 0 0 0).

Momenta	$\Gamma(0, 0, 0)$	$A(0, 0, \pi)$	$M(\pi, 0, 0) \times 3$	$L(\pi, 0, \pi) \times 3$
parities	+, +	+, -	+, -	+, -
produce	(+)	(-)	(-)	(-)

TABLE I: The parities of the occupied bands at the time-reversal invariant momenta for hcp Be and the products of the parities for the two occupied bands.

To further elucidate the topological feature in beryllium, we have also constructed a 2×2 Hamiltonian within the framework of the low-energy $k \cdot p$ model in describing two bands

crossing, briefly. Using the $|s\rangle$ and $|p\rangle$ states as the bases, respecting time-reversal, and D_{6h} symmetries, the model Hamiltonian around Γ can be written as,

$$H_{\Gamma}(\mathbf{k}) = \epsilon(\mathbf{k}) + \begin{pmatrix} M(\mathbf{k}) & B(\mathbf{k}) \\ B^{\dagger}(\mathbf{k}) & -M(\mathbf{k}) \end{pmatrix} \quad (3)$$

where

$$\epsilon(\mathbf{k}) = \epsilon_0 + a_{\parallel}(k_x^2 + k_y^2) + a_{\perp}k_z^2 \quad (4)$$

$$M(\mathbf{k}) = m_0 + m_{\parallel}(k_x^2 + k_y^2) + m_{\perp}k_z^2 \quad (5)$$

$$B(\mathbf{k}) = B_0k_z \quad (6)$$

and the eigenvalues of the model Hamiltonian are $E(\mathbf{k}) = \epsilon(\mathbf{k}) \pm \sqrt{M^2(\mathbf{k}) + B^2(\mathbf{k})}$. In this case, the gapless solutions of Equ. (3), at which the Dirac node line would appear, can be yielded only when both $M(\mathbf{k})$ and $B(\mathbf{k})$ equal zero. Within this condition, on the $k_z=0$ plane the node line locates at $|\mathbf{k}| = \pm \sqrt{-\frac{m_0}{m_{\parallel}}}$ which requires $m_0 m_{\parallel}$ is always smaller than zero. This is also the condition of the band inversion occurrence. With other words, when band inversion happens, in the lack of SOC, there always exists a node line in the momentum space, which are the solutions of $M(\mathbf{k}) = B(\mathbf{k}) = 0$. Noted that the band inversion only occurs at Γ among all TRIMs for Be according to the abovementioned topology analysis, a Dirac node line would occur around the Γ point in agreement with the calculated electronic structure.

Using this Hamiltonian to describe the (0001) surface bands, the topologically nontrivial surface states could be expected. Since the (0001) surface is perpendicular to c -axis, we can use $-i\partial_z$ instead of k_z according to the theory to the linear order and then the (0001) surface Hamiltonian can be expressed as follows,

$$H_{\Gamma}^{surf}(\mathbf{k}) = \epsilon_0 + a_{\parallel}k^2 + \begin{pmatrix} m_0 + m_{\parallel}k^2 & -iB_0\partial_z \\ iB_0\partial_z & -m_0 - m_{\parallel}k^2 \end{pmatrix} \quad (7)$$

Due to the Jackiw-Rebbi problem [40], there will be a topological boundary mode with the condition of $m_0 + m_{\parallel}k^2 < 0$. This suggests the presence of the topologically nontrivial surface states, which would nestle the projected Dirac node ring. To clarify this point, we calculate the surface electronic structures by varying the thickness of the slab as shown in Fig. 3a-3f. As expected, the robust surface electronic bands (SF-band 1 in Fig. 3f) appear, when the slab's thickness is above five unit cells along the c -axis. As shown in Fig. 3f, from the crossing A to B point the topological surface bands are two-fold degenerated within the projected Dirac node ring. It can be seen that the topological surface bands along the \bar{K} - $\bar{\Gamma}$ - \bar{M} direction disperse parabolically from the lowest energy of -2.73 eV (expt[26, 38]: -2.80 eV and -2.75 eV, referred to the Fermi level) at $\bar{\Gamma}$, and then cross the Fermi level at 47% (expt[38]: 49%) of the $\bar{\Gamma}$ - \bar{K} distance and 64% (expt[38]: 58%) of the $\bar{\Gamma}$ - \bar{M} distance, in nice agreement with the experimental

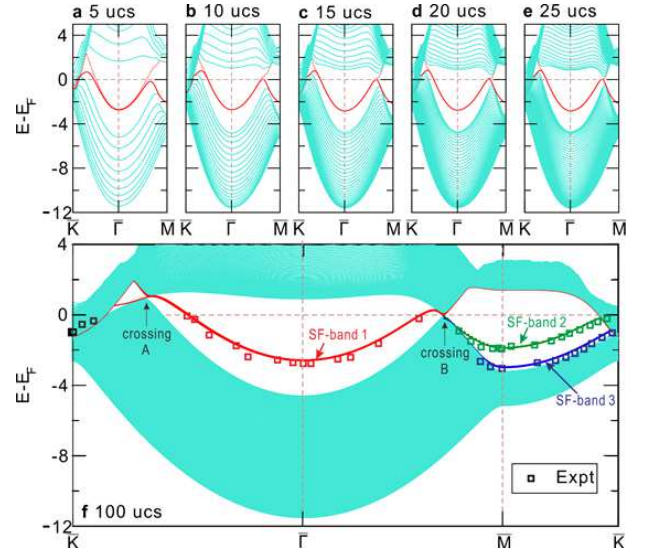


FIG. 3: The evolution of thickness-dependent surface electronic band structures of the Be (0001) surface. a to e, the derived surface electronic structure is shown as a function of the slab thickness from 5 unit cells (ucs) to 25 ucs along c -axis with an increasing of 5 ucs thickness of every image. It can be seen that, with increasing the thickness, the surface states (red curves) almost remains unchanged and the bands touch more closely at both crossing A and B points, which correspond to the band crossing points projected by the bulk energy bands. f, Surface electronic band structure with a slab thickness of 100 ucs, together with the experimentally measured data (squares[26]).

findings (see squares in Fig. 3f) obtained by ARPES[26, 38]. Particularly, it has been noted that the surface bands around the $\bar{\Gamma}$ and \bar{M} points are highly different. The topologically protected SF-band 1 around the $\bar{\Gamma}$ point are mainly comprised with s and p_z -like electronic states from the topmost atomic layer, reflecting well the crucial feature of the band inversion between s and p_z in its bulk phase (Fig. 1c). This SF-band 1 is indeed half-filled when the surface is electrically neutral. The other two surface bands around \bar{M} (SF-band 2 and 3 in Fig. 3f) are the topologically trivial states, which are not correlated with the DNL state. The SF-band 2 is mainly composed with in-plane $p_{x,y}$ -like electronic states from the topmost surface atomic layer, whereas the SF-band 3 mainly consists of the $p_{x,y}$ -like electronic states from the second outer atomic layer. Obviously, these SF-bands 2 and 3 are fully occupied when the surface is electronic neutral.

We have further derived its Fermi surface of the (0001) surface in Fig. 4a. Because the DNL exists on the $k_z = 0$ plane in the BZ, the DNL projection onto the (0001) surface shows a closed circle (Ring A in Fig. 4a) surrounding $\bar{\Gamma}$ within which the topologically protected surface bands (Ring B in Fig. 4a) appear. Although the Ring B was already observed by ARPES[38] (Fig. 4b and 4c), it was not interpreted as the DNL-induced topologically non-trivial bands. The understanding of the surface states (SF-band 1 in Fig. 3f and Ring B in Fig. 4a) has also been a long-standing question since the

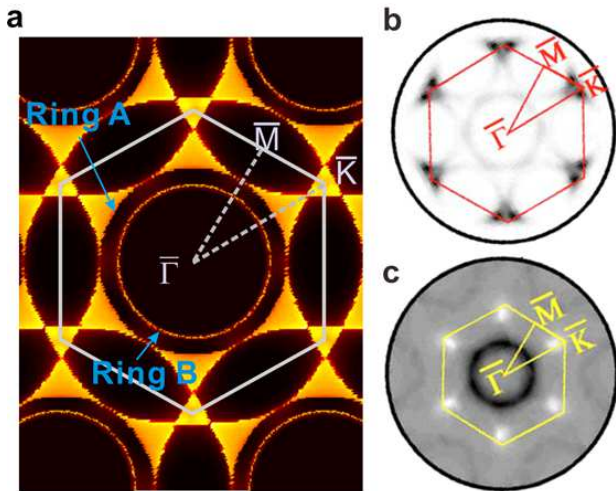


FIG. 4: **Fermi surface of the Be (0001) surface.** **a**, DFT-derived Fermi surface highlighting a surface state of a fully closed circle around the centered Γ point in the Brillouin zone. The other parts are the projections of bulk bands. **b** and **c**, the experimentally measured Fermi surface cuts with $h\nu = 32.5$ eV and 86 eV, respectively, showing the difference between horizontal and vertical polarizations measured by the ARPES experiments. The panels **(b)** and **(c)** are directly adopted from the experimental report[38].

1980s[26–34]. It was suspected to be correlated with unusually large outward relaxation of the topmost surface atoms, so-called p to s electron demotion as well as the core-level shifts[26–28, 32–34]. However, those proposed mechanisms did not address the underlying physical origin for the appearance and stability of the surface states[26]. Due to our calculations, the SF-band 1 state is highly robust, no matter whether the surface slab modeling are relaxed or not (Supplementary Materials). Therefore, it is undoubtable that the SF-band 1 is induced by the topological DNL feature in its bulk phase. Looking back on the unusual physics properties of Be (0001) surface, the puzzlings can be rationalized by the presence of topologically non-trivial DNL states. The DNL induced topological surface bands would certainly behave far beyond the nearly-free-electron model, and the nearly flat dispersion of them results in very large electron density of state nearby the Fermi level of (0001) surface, which would cause giant electron-phonon coupling effect and Friedal oscillations. Additionally, we would like to mention that, as early as in 1970, the Landau quantum oscillations of the magnetic susceptibility has been observed when the magnetic field was set to be parallel to the c -axis direction[41]. This seems to be another exciting sign to elaborate the DNL property in Be because the magnetic field certainly breaks the time-reversal symmetry and gap out the crossings to modify the Fermi surface.

Finally, we have also found the similar topological DNL feature in Mg, Ca and Sr. Mg is isostructural and isovalent to Be and their electronic band structures look highly similar to each other. In Mg (which is similar to Be) there also exists a DNL around the Fermi level and, the topologically protected

non-trivial surface states are also obtained on (0001) surface by surface calculations, which are also in nice agreement with experiments(Supplementary Materials). Metals of Ca and Sr, which are isovalent to Be and Mg, crystallize in fcc structure with the truncated-octahedron Brillouin zone. These two metals also exhibit the DNL-like topological feature. On each hexagonal face of the Brillouin zone, the valence and conduction bands cross each other to form a closed loop which surrounds the center of the hexagonal face. Topological surface states can also be observed clearly on their symmetrically equivalent $\{111\}$ surfaces. However, different from Be their topological surface bands locate outside the projected DNLs because the band inversion occurs outside the DNLs.

In summary, through first-principle calculations, we propose that 3D topological DNL semimetal states can be obtained in pure alkali earth metals of beryllium, magnesium, calcium and strontium. The anomalous topological surface bands are obtained on the (0001) surface of Be (and Mg), and in nice agreement with previous experimental observations. This fact confirms that the previous observed anomalous electron behaviors on Be (0001) surface should be induced by the topological non-trivial DNL state in its bulk and rationalize a series long-standing puzzling physical properties on its (0001) surface. The perfect agreement of physical properties between theoretical predictions of DNL semimetals and experimental observations on Be (0001) surface makes beryllium a good platform for researching topological DNL semimetals. On the other hand, the discovery of DNL states in alkali earth metals implies that this fascinating topological property might also exist in other elemental metals, supporting a new direction for designing topological DNL semimetals.

Acknowledgments We thank R. H. Hao for comments and polishing in English on the manuscript. This study was supported by the 'Hundred Talents Project' of the Chinese Academy of Sciences and from the Major Research Plan (Grant No. 91226204), the Key Research Program of Chinese Academy of Sciences (Grant No. KGZD-EW-T06), the National Natural Science Foundation of China (Grant Nos. 51474202 and 51174188) and the Beijing Supercomputing Center of CAS (including its Shenyang branch) as well as the high-performance computational cluster in the Shenyang National University Science and Technology Park.

* Corresponding author: xingqiu.chen@imr.ac.cn

- [1] M. Z. Hasan, S.-Y. Xu, and G. Bian. Phys. Scr., T**164**, 014001 (2015).
- [2] S. M. Young, S. Zaheer, J. C. Y. Teo, C. L. Kane, E. J. Mele and A. M. Rappe. Phys. Rev. Lett. **108**, 140405 (2012).
- [3] X. Wan, A. M. Turner, A. Vishwanath, and S. Y. Savrasov. Phys. Rev. B, **83**, 205101 (2011).
- [4] S. Ryu, and Y. Hatsugai. Phys. Rev. Lett. **89**, 077002 (2002).
- [5] T. T. Heikkilä, G. E. Volovik. JETP Lett. **93**, 59 (2011).
- [6] A. A. Burkov, M. D. Hook, and L. Balents. Phys. Rev. B, **84**, 235126 (2011).

- [7] Z. J. Wang, Y. Sun, X.-Q. Chen, C. Franchini, G. Xu, H. M. Weng, X. Dai and Z. Fang. *Phys. Rev. B*, **85**, 195320 (2012).
- [8] Z. K. Liu, B. Zhou, Y. Zhang, Z. J. Wang, H. M. Weng, D. Prabhakaran, S. K. Mo, Z. X. Shen, Z. Fang, X. Dai, and Z. Hussain. *Science*, **343**, 864-867 (2014).
- [9] X. Y. Cheng, R. H. Li, Y. Sun, X.-Q. Chen, D. Z. Li, and Y. Y. Li. *Physical Review B*, **89**, 245201 (2014).
- [10] S. Y. Xu, C. Liu, S. K. Kushwaha, R. Sankar, J. W. Krizan, I. Belopolski, M. Neupane, G. Bian, N. Alidoust, T. R. Chang, H. T. Jeng, C. Y. Huang, W. F. Tsai, H. Lin, P. P. Shibayev, F. C. Chou, R. J. Cava, and M. Z. Hasan. *Science*, **347**, 294-298 (2015).
- [11] Z. J. Wang, H. M. Weng, Q. S. Wu, X. Dai, and Z. Fang. *Phys. Rev. B*, **88**, 125427 (2013).
- [12] M. Neupane, S. Y. Xu, R. Sankar, N. Alidoust, G. Bian, C. Liu, I. Belopolski, T. R. Chang, H. T. Jeng, H. Lin, A. Bansil, F. Chou, and M. Z. Hasan. *Nature Communications*, **5**, 3786 (2014).
- [13] Z. K. Liu, J. Jiang, B. Zhou, Z. J. Wang, Y. Zhang, H. M. Weng, D. Prabhakaran, S. K. Mo, H. Peng, P. Dudin, T. Kim, M. Hoesch, Z. Fang, X. Dai, Z. X. Shen, D. L. Feng, Z. Hussain and Y. L. Chen. *Nature Materials*, **13**, 677-681 (2014).
- [14] H. M. Weng, C. Fang, Z. Fang, B. A. Bernevig, and X. Dai. *Phys. Rev. X*, **5**, 011029 (2015).
- [15] S. M. Huang, S. Y. Xu, I. Belopolski, C. C. Lee, G. Q. Chang, B. K. Wang, N. Alidoust, G. Bian, M. Neupane, C. L. Zhang, S. Jia, A. Bansil, H. Lin, and M. Z. Hasan. *Nature Communications*, **6**, 7373 (2015).
- [16] B. Q. Lv, H. M. Weng, B. B. Fu, X. P. Wang, H. Miao, J. Ma, P. Richard, X. C. Huang, L. X. Zhao, G. F. Chen, Z. Fang, X. Dai, T. Qian, and H. Ding. *Phys. Rev. X*, **5**, 031013 (2015).
- [17] S. Y. Xu, I. Belopolski, N. Alidoust, M. Neupane, G. Bian, C. L. Zhang, R. Sankar, G. Q. Chang, Z. J. Yuan, C. C. Lee, S. M. Huang, H. Zheng, J. Ma, D. S. Sanchez, B. K. Wang, A. Bansil, F. C. Chou, P. P. Shibayev, H. Lin, S. Jia, and M. Z. Hasan. *Science*, **349**, 613-617 (2015).
- [18] A. A. Soluyanov, D. Gresch, Z. J. Wang, Q. S. Wu, M. Troyer, X. Dai, and B. A. Bernevig. *Nature*, **527**, 495-499 (2015).
- [19] H. M. Weng, Y. Y. Liang, Q. N. Xu, R. Yu, Z. Fang, X. Dai, and Y. Kawazoe. *Phys. Rev. B*, **92**, 045108 (2015).
- [20] R. Yu, H. M. Weng, Z. Fang, X. Dai, and X. Hu. *Phys. Rev. Lett.*, **115**, 036807 (2015).
- [21] Y. Kim, B. J. Wieder, C. L. Kane, and A. M. Rappe. *Phys. Rev. Lett.*, **115**, 036806 (2015).
- [22] L. S. Xie, L. M. Schoop, E. M. Seibel, Q. D. Gibson, X. X. Xie, and R. J. Cava. *APL Materials*, **3**, 083602 (2015).
- [23] M. G. Zeng, C. Fang, G. Q. Chang, Y.-A. Chen, T. Hsieh, A. Bansil, H. Lin, and L. Fu. arXiv: 1504.3492 (2015).
- [24] L. Lu, L. Fu, J. D. Joannopoulos, and M. Soljačić. *Nature Photonics*, **7**, 294-299 (2013).
- [25] K. Mullen, B. Uchoa, and D. T. Glatzhofer. *Phys. Rev. Lett.*, **115**, 026403 (2015).
- [26] E. W. Plummer, and J. B. Hannon. *Progress in Surface Science*, **46**, 149-158 (1994).
- [27] U. O. Karlsson, S. A. Flodstrom, R. Engelhardt, W. Gadeke, and E. E. Koch. *Solid State Commun.*, **49**, 711-714 (1984).
- [28] R. A. Bartynski, E. Jensen, T. Gustafsson, and E. W. Plummer. *Phys. Rev. B*, **32**, 1921-1926 (1985).
- [29] M. Hengsberger, D. Purdie, P. Segovia, M. Garnier, and Y. Baer. *Phys. Rev. Lett.*, **83**, 592-595 (1999).
- [30] T. Y. Chien, X. B. He, S.-K. Mo, M. Hashimoto, Z. Hussain, Z.-X. Shen and E. W. Plummer. *Phys. Rev. B*, **92**, 075133 (2015).
- [31] P. T. Sprunger, L. Petersen, E. W. Plummer, E. Laegsgaard, and F. Besenbacher. *Science*, **275**, 1764-1767 (1997).
- [32] H. L. Davis, J. B. Hannon, K. B. Ray, and E. W. Plummer. *Phys. Rev. Lett.*, **68**, 2632-2635 (1992).
- [33] L. I. Johansson, H. I. P. Johansson, J. N. Andersen, E. Lundgren, and R. Nyholm. *Phys. Rev. Lett.*, **71**, 2453-2456 (1993).
- [34] P. J. Feibelman. *Phys. Rev. B*, **46**, 2532-2539 (1992).
- [35] N. Marzari, D. Vanderbilt, A. De Vita, M. C. Payne. *Phys. Rev. Lett.* **82**, 3296(1999).
- [36] J.-H. Cho, Ismail, Z. Y. Zhang, E. W. Plummer. *Phys. Rev. B*, **59**, 1677(1999).
- [37] M. Y. Chou, P. K. Lam, M. L. Cohen. *Phys. Rev. B*, **28**, 4179-4185 (1983).
- [38] I. Vobornik, J. Fujii, M. Mulazzi, G. Panaccione, M. Hochstrasser, and G. Rossi. *Phys. Rev. B*, **72**, 165424 (2005).
- [39] L. Fu, C. L. Kane, and E. J. Mele. *Phys. Rev. Lett.* **98**, 106803 (2007).
- [40] R. Jackiw, and C. Rebbi. *Phys. Rev. D*, **13**, 3398-3409 (1976).
- [41] L. R. Testardi, and J. H. Condon. *Phys. Rev. B*, **1**, 3928-3942 (1970).